Available online at www.sciencedirect.com

ScienceDirect

Progress in Natural Science: Materials International 24 (2014) 42–49

Progress in Natural Science Materials International

www.elsevier.com/locate/pnsmi
www.sciencedirect.com

Original Research

Preparation and characterization of polypropylene/silica composite particle with interpenetrating network via hot emulsion sol–gel approach

Lei Zu[a,b], Ruirui Li[b], Longyi Jin[a], Huiqin Lian[b], Yang Liu[b], Xiuguo Cui[a,b,*]

[a]*Department of Chemistry, Yanbian University, Yanji 133002, China*
[b]*Beijing Key Lab of Special Elastomer Composite Materials, Department of Material Science and Engineering, Beijing Institute of Petrochemical Technology, Beijing 102617, China*

Received 14 July 2013; accepted 4 November 2013
Available online 14 February 2014

Abstract

A novel interpenetrating structural ultrafine polypropylene-silica nanocomposite particles were synthesized by a modified sol–gel approach in the presence of the melt polypropylene emulsion. A series of samples with different polypropylene content was prepared to investigate the unique characteristics of this original nanocomposite. The thermal gravimetric analysis and differential scanning calorimetry results showed that the nanocomposites had the interpenetrating structure and good thermal stability, and the crystallization behavior of polypropylene was confined by the silica matrix. The interpenetrating structure of nanocomposites was also suggested by the nitrogen adsorption–desorption measurement results. The scanning electronic microscope and transmission electron microscopy images indicated that the nanocomposites had irregular particle morphology. The nanoparticle tracking analysis results show that the mean size of the nanocomposites was around 160 nm. According to the results obtained from different measurements, a reasonable formation mechanism was proposed.

Keywords: Polypropylene; Silica; Nanocomposites; Sol–gel method; Interpenetrating structure

1. Introduction

In recent years, the organic-inorganic composite materials based on organic polymers and silica have been studied widely for their potential applications in optics [1–4], functional materials [5], and biosciences [6–9]. A series of organic-silica composite materials were designed for a variety of structures to meet different application requirements [10–12]. Among these different structural materials, the interpenetrating structural composite materials, the polymer–silica 3D networks are held together by permanent entanglement, have attracted much attentions for their excellent characterizes [13–15].

Recently, many researchers have synthesized various polymer–silica composites via different approaches. For example, Gabriela Bonilla etc. synthesized the ternary interpenetrating networks of polyurethane-poly(methyl methacrylate)-silica by the in-situ bulk polymerization [16]. Tomoki Ogoshi and Yoshiki Chujo prepared a highly transparent and homogeneous poly(vinylidene fluoride)-silica composite material by the in-situ interpenetration polymer network method [17]. Chang Hyun Lee etc. synthesized the sulfonated polyimide-silica containing interpenetrating polymer network through a complicated consecutive two-step synthetic method [18]. Isam M. Arafa etc. prepared the urea-formaldehyde-silica composites by the sol–gel method [19].

However, it is notable that, although many diverse organic polymers were chosen to form the interpenetration structural composite materials, but some widely used polymers which possess unique characterizes, such as polypropylene (PP) and polycarbonate have not been found yet.

Polypropylene is one of the commonly used polymers composed of linear $[-CH_2CH(CH_3)-]_n$ chains. Compared with the other polymers, the polypropylene has a great potential for various applications because of its many desirable properties, especially the low density, high melting temperature, good

*Corresponding author. Tel./fax: +86 10 81294007.
E-mail address: cuixiuguo@bipt.edu.cn (X. Cui).
Peer review under responsibility of Chinese Materials Research Society.

Production and hosting by Elsevier

1002-0071/$ - see front matter © 2014 Chinese Materials Research Society. Production and hosting by Elsevier B.V. All rights reserved.
http://dx.doi.org/10.1016/j.pnsc.2014.01.001

mechanical strength and thermal stability, superior solvent resistance and low cost. The incorporation of PP and silica may result in significant improvements in the properties of the composites compared with virgin polymer and silica. These improvements include increased mechanical strength and elastic modulus, improved heat and flame resistance, reduced gas permeability and increased biodegradability [20]. These properties have led to the application of polypropylene-silica composites in various industrial fields, e.g., the automotive, packaging, cell, medical and technical textile industries [21–23].

Commonly, the PP–SiO_2 composite materials could be prepared through simply mixing the silica and PP. However, this approach could not obtain a good dispersion of the silica or PP due to the significant difference of the interfacial adhesion characters between the PP and silica, and hence the expected exceptional characterizes of the composites may not be obtained. In order to improve the interfacial adhesion, there has been particular interest in composites of this type in which the PP is constrained within the pores of silica, sometimes down to the molecular level. Therefore, the PP–SiO_2 composites were usually synthesized to the nanocomposites with the core–shell or interpenetrating structures. In such nanocomposites, stable chemical crosslinking and/or ordered physical entanglement exist among PP and silica.

Compared with the other polymer–silica composites, the PP–silica nanocomposites with the interpenetrating structure have a chance to possess some special characterizes. Firstly, the interpenetrating structure may prevent the phase separation between PP and silica, which lead to a well stability during the preparation and application. With the merit of this characterize, the PP–SiO_2 nanocomposites could be used as the filler to improve the mechanical strength of the blend which is commonly prepared by simply mixing the silica and PP. Secondly, the PP–SiO_2 nanocomposites are natural amphipathic due to the interval distribution of the hydrophilic and hydrophobicity, and hence they may have a chance to be utilized as the hydrophobic interaction chromatography materials [24,25]. Moreover, the PP–SiO_2 nanocomposites have a good biocompatibility due to the nontoxicity of PP and silica. Thus, the PP–SiO_2 nanocomposites could be utilized as the medicine carrier in biological pharmacy field. Thirdly, the toughness of silica in PP–SiO_2 nanocomposites would be enhanced by PP and lead to a possibility of being used in lithium cells as the cathode material. Usually, the cathode materials which are made of silica in lithium cells are easy to be destroyed during the application due to the fragility of silica [26,27]. Therefore, the silica cathode materials are needed to be toughened for improving their performance. Although many polymers could be used as the candidate to fulfill this work, but PP may be regarded as the best one owing to the well toughness and a higher melting temperature compared with the other polymers.

Accordingly, from all the potential applications mentioned above, it is easy to find out the PP is an ideal candidate to form polymer–silica nanocomposites and the preparation and utilization of interpenetrating structural PP–SiO_2 nanocomposites possess a very high research value both in academic and industry.

However, the nature characterization of the PP brings it a lot of challenges to be composited with the silica. In fact, the PP–SiO_2 nanocomposites could not be synthesized by using the general methods, such as the emulsion polymerization, dispersion polymerization or the common sol–gel method due to the immense difficulty of finding a fine solvent and effective emulsify to make a stable PP emulsion in ambient temperature. Consequently, a special approach should be applied to synthesize the interpenetrating structural PP–SiO_2 nanocomposites. In the present investigation, the novel interpenetrating structural ultrafine PP–silica nanocomposite particles were synthesized through the modified sol–gel method in the presence of the PP emulsion. A series of samples with different PP content was synthesized to investigate the unique characteristics of the original nanocomposits. Based on the different test results, a reasonable formation mechanism was also proposed. The morphology and structure information of the nanocomposites were characterized by the scanning electronic microscope (SEM), transmission electron microscopy (TEM). The mean size and size distribution were measured by the nanoparticle tracking analysis (NTA). The thermal and crystallization behavior were determined by the thermal gravimetric analysis (TGA), differential scanning calorimetry (DSC) measurements and X-ray diffraction (XRD) analysis. The specific surface area, mean pore volume and mean pore size of the nanocomposites were measured by the nitrogen adsorption–desorption measurements.

2. Experimental procedure and characterization

2.1. Materials

Polypropylene (melting index of 12.3 g/10 min), tetraethyl orthosilicate (TEOS), xylene, and ammonium hydroxide were purchased from Beijing Chemical Reagents Company, China. Polyethylene-block-poly(ethylene glycol) (PE-b-PEG, Mw 1400, PE/PEG 1:1 by weight) was obtained from Sigma-Aldrich. All chemicals are analytical reagent and used as received without any further purification.

3. Experimental method

In a typical procedure, 4 mL boiling xylene was added to a melting mixture of 0.2 g PP and 1.3 g PE-b-PEG and stirred vigorously at 140 °C for 2 h. Then 10 ml TEOS was added and stirred until a clear solution (hydrophobic phase) was obtained. The hydrophobic solution was then poured into a boiling hydrophilic solution, 50 mL ethanol/30 mL ammonium hydroxide solution (25% by weight of NH_3), and stirred at 78 °C for 30 min to form a stable emulsion. Then the emulsion was cooled and stirred at 25 °C for 24 h. After the reaction, the resulting dispersion was centrifuged at 10,000 rpm for 20 min. The precipitate was washed with ethanol twice, and dried at 100 °C for 10 h.

To evaluate the correlation between the PP content and the mean size of the PP–SiO_2, the products with different mass ratio of PP to xylene (2 wt%, 3 wt% and 6 wt%) were synthesized by the same procedure mentioned above and the products were named S1, S2 and S3 successively. The products were calcined for 2 h at 200 °C, 400 °C and 550 °C respectively for obtaining more details of the structure information.

3.1. Characterization

The size distributions of the PP–SiO_2 were measured by the nanoparticle tracking analysis (NTA, NanoSight LM20). The NTA is a powerful tool to obtain the average statistical data of the sample′s dimension, which based on the correlation between the sample size and the corresponding Brownian motion velocity under a certain temperature and viscosity of the disperse phase [28]. In this study, the disperse phase was ultrapure water, with 20 °C. The morphology observation was performed with FEI QUANTA-400F scanning electronic microscope (SEM), operating at 20 kv and transmission electron microscopy (TEM, Philips CM12, operating at 200 KeV). Surface area and porosity analysis were measured by the nitrogen adsorption–desorption experiments. The thermal properties were measured on TA Instrument Q500 thermal gravimetric analysis (TGA), nitrogen atmosphere, 10 °C/min, and TA Instrument Q2000 differential scanning calorimetry (DSC), nitrogen atmosphere, 10 °C/min. Wide-angle X-ray scattering (WAXS) analysis was performed with SHIMADZU XRD-7000, using Cu-Kα radiation ($\lambda = 0.154$ nm) at 40 kV and 30 mA.

4. Results and discussion

The most important factor for the preparation is the choice of the surfactant to make a stable emulsion. A wide variety of surfactants had been tested, including the anionic surfactants sodiumdodecylsulfate (SDS), the cationic cetyltrimethylammonium bromide (CTAB) and the non-ionic Span 80, Tween 20 and PE-b-PEG. Among of these surfactants, only the PE-b-PEG could make a stable PP emulsion. The PE-b-PEG is a block copolymer which provides a HLB ratio of 10, making it suitable for the formation of O/W emulsions. The structure of PE-b-PEG is $H_3CH_2C(CH_2CH_2)_{25}(OCH_2CH_2)_{16}OH$. The PEG block is highly compatible with the water alcohol phase in the middle temperature (50–80 °C), and the PE block is suitable for the oil phase due to the structure and property of PE are similar with the PP. Interestingly, it is noticed that the emulsion mentioned above was not stable by only using the PE-b-PEG as the surfactant, which may be due to the PE block do not have enough compatibility with the PP. However, when TEOS was used along with the PE-b-PEG, a relative stable emulsion could be obtained, so it could be inferred that the TEOS may possess some emulsification and played the co-surfactant role in the reaction. This conclusion is consistent with the report of Che et al. [29] that the oleic acid emulsion droplets acted as the template to synthesize the mesoporous hollow silica spheres. They have found that after addition of 3-aminopropyltriethoxysilane (APES) and TEOS, the oil droplets were slowly emulsified by APES and TEOS and the size of the oil droplet/co-structure directing agent (CSDA)/silica species composite was gradually decreased to several nanometers. According to this result, it is reasonable to infer that the TEOS may play a similar emulsification in this research.

Fig. 1 shows the particle size distribution of the PP–SiO_2. It can be observed that the particle size distribution of PP–SiO_2 (S1) is relatively broad, from 60 nm to 300 nm. With increasing the PP content, the particle size became more uniform although the particle size distribution was not changed too much. There are four distribution peaks could be observed in S2 and only two distribution peaks emerged in S3. These results show that the particle size distribution is affected by the content of PP. The particle size distribution became more uniform when more PP was added. However, it is notable that the distribution of particle size presents a certain extent multiple relationship. This multiple relationship could be attributed to the adhesion and/or aggregation among the particles. Commonly, the condensation of the TEOS is too fast to make a regular and well-proportioned self-assembly process under the alkaline condition, so the adhesion and aggregation would occur among the particles, and the bigger particles are usually composed of two or more small particles. Therefore, the multiple relationship of particle size was presented.

The mean particle size of PP–SiO_2 could also be obtained by NTA measurements. The mean particle sizes of S1, S2 and S3 were 150 nm, 168 nm and 172 nm respectively. It should be mentioned that the mean particle size obtained by NTA measurement is a statistical number which was calculated from a great number of particles, the density of particles tested in this paper was more than 10^6 particles/ml, therefore the mean particle size has a more average meaning. According to these particle size distribution and mean particle size results, it is reasonable to infer that the PP content would determine the mean size and uniformity of PP–SiO_2 to a certain extent. It has been found that the more PP was added, the more uniform and bigger mean size PP–SiO_2 particles could be obtained.

The SEM observations of the PP–SiO_2 (S3) are presented in Fig. 2A and B. The surface morphology of the PP–SiO_2 shows that the nanocomposites were composed of particles of different shapes and sizes. These is no polymer that could be observed outside the particles, indicating that the polymer was located within the silica. It can be seen clearly that the particles possessed a non-uniform aggregation, some smaller particles were adhered together to form a big one, which could prove the multiple relationship of particle size, as shown in Fig. 1. Commonly, the hydrolysis and condensation of TEOS are reported to promote the formation of a cross-linked structure [30]. Therefore, the aggregations of particles could be attributed to the irregular self-assembly of TEOS. In addition, the relative high synthesis temperature would also disturb the self-assembly process of TEOS. It should be mentioned that some stripes could be observed on the surface of the particles. These stripes may be composed by silica, proved by the similar

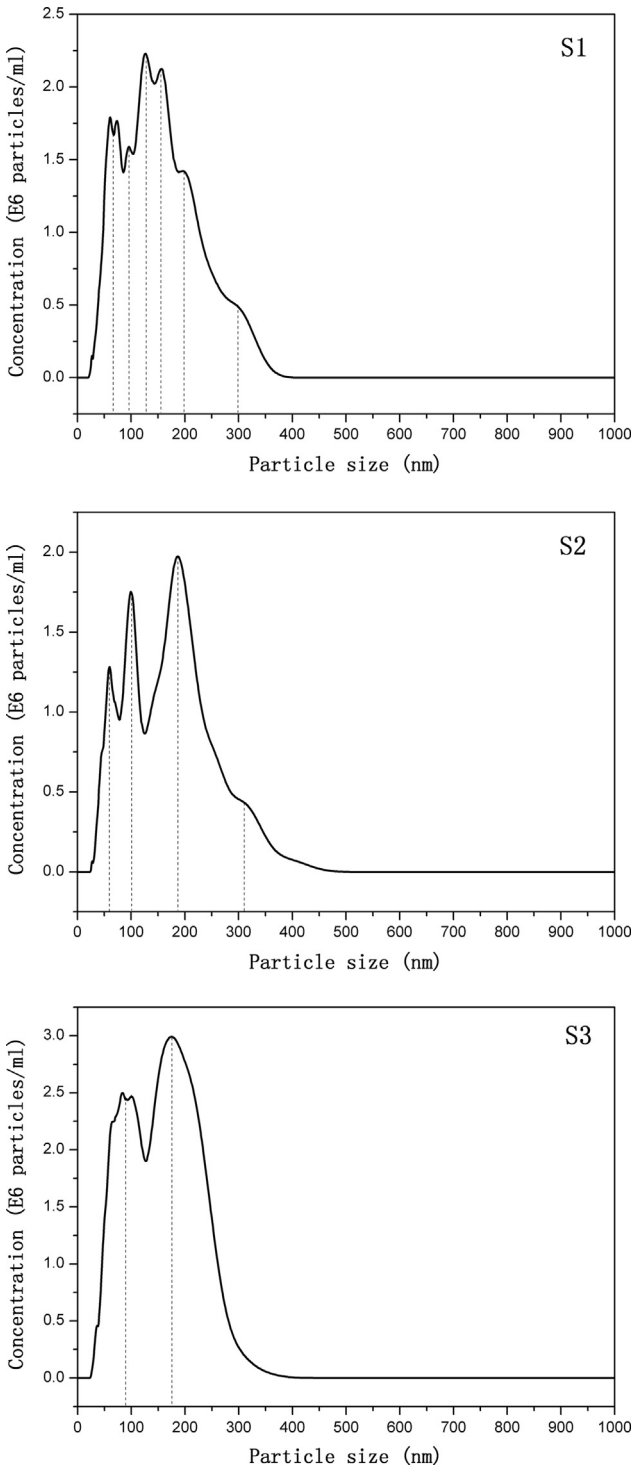

Fig. 1. Particle size distribution of the PP–SiO_2.

contrast with the silica matrix, as can be seen in Fig. 2C and D. The formation process of these silica stripes may be related to the interaction between TEOS and PE-b-PEG.

As the surfactant, the PEG block of the PE-b-PEG is hydrophilic, when the TEOS was hydrolyzed, since the O atom electronegativity of PEG block is stronger than that of the hydroxyl group, and the number is also much larger than that, the hydrolysis products prefer to interact with the O atom in PEG block by the attraction of opposite charges instead of the hydroxyl group. Therefore, the hydrolysis products of TEOS prefer inhabiting around the O atom in PEG block and formed a silica network to interact with the hydroxyl group at the end of the PEG block, which formed the irregular stripes on the surface of PP–SiO_2. Furthermore, for obtaining a stable emulsion, much excess TEOS were added in the oil phase, after the oil phase was poured into the water phase, only a part of TEOS would stay in the oil drop as the co-surfactant and the others would distribute in the water phase. So the hydrolysis and condensation products of TEOS in the water phase may be also attached on the silica matrix or form the conjoint silica residue among the particles.

The TEM images present the structure information of PP–SiO_2. As shown in Fig. 2C and D, the adherence between the particles could be observed clearly. There is no typical hollow structure could be observed among the particles, indicating the PP–SiO_2 was not the core–shell structure. Considering that the polymer was located within the silica, as suggested by SEM images, it is reasonable to infer that the PP–SiO_2 may possess an interpenetrating structure, which confirmed by the TGA, DSC and nitrogen adsorption–desorption measurement results.

The thermal properties of the PP–SiO_2 (S3), PE-b-PEG and PP are shown in Fig. 3. From the TGA (curve I) and DTG (curve II) curves of the PP–SiO_2 (Fig. 3A), it can be seen clearly that four weight decrease stages could be observed in PP–SiO_2, the first one may be caused by the evaporation of water and ethanol, and the second stage could be assigned to the existence of xylene (the boiling point is about 140 °C), the third and fourth stages could be attributed to the pyrolysis of PE-b-PEG (about 60% of total mass decrease) and PP (about 10% of total mass decrease) respectively. Compared with the neat PP, the decomposition temperature of PP in PP–SiO_2 was increased dramatically, from 425 °C to 490 °C, indicating that the thermal decomposition of PP was strongly restricted by silica walls.

Fig. 3B shows the DSC profiles of PP–SiO_2 (S3), PE-b-PEG and neat PP. As presented in Fig. 3B, there are two endotherm peaks could be observed in PE-b-PEG. The endotherm peak at around 51 °C corresponding to the melting transition of crystalline PEG, and the endotherm peak at around 103 °C could be assigned to the crystalline PE. The endotherm peak of neat PP emerged at around 151 °C. It is notable that the melting transition of PEG had largely vanished in S3, which suggests that so much of the PEG was constrained that crystallization was essentially thwarted. This result is consistent with the previous reports [31,32] that the characteristic bulk glass transition temperature of polymer disappeared when the chains were penetrated into the pores of a mesoporous silica. Therefore, it could be inferred that the PEG in PE-b-PEG had penetrated into the silica pores. The absence of a bulk glass transition was attributed to the confinement of the polymer chains interfering with the thawing of long-range motions characteristic of the non-glassy state. In the case of the melting points, the confinement may prevent the formation of sufficiently large nuclei to survive, rather than remelt [33]. Similarly, as can be seen in S3, the melting temperature of PP

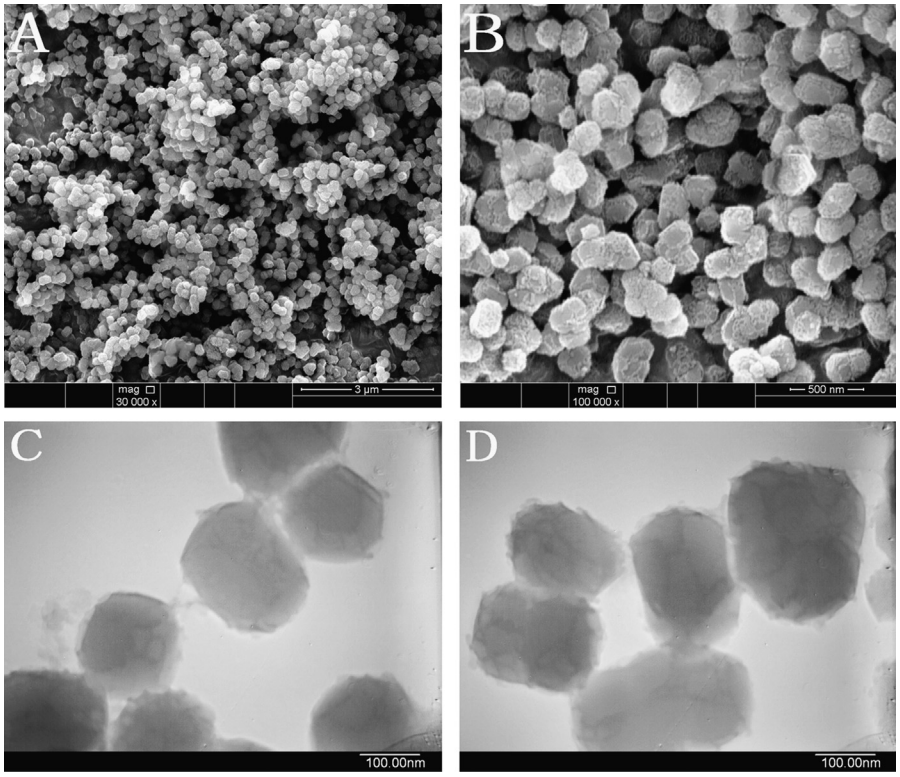

Fig. 2. Morphology of the PP–SiO_2. (A and B) SEM images of S3. (C and D) TEM images of S3.

in PP–SiO_2 decreased more than 10 °C compared with the neat PP. This result could also be explained by the restriction of silica. As the similar conclusion from Jackson et al. [34,35], when molecules were confined to dimensions not much more than several times their average size, their glass transitions were lowered. Therefore, it is reasonable to infer that the PP had also penetrated into the silica pores.

The proximate degree of crystallinity of PP in PP–SiO_2 could be evaluated from the DSC measurements. The degree of crystallinity of PP in PP–SiO_2 is estimated to be 10.5%, based on the melting heat value of 21.65 g/J and the usually assumed specific melting heat value of 207 g/J for extrapolated the theoretical crystalline PP. This relative low crystallinity manifests that the crystallization behavior of PP was confined by the silica. The results obtained from the TGA and DSC measurements demonstrate that the PP was entrapped by the silica matrix and the silica wall confined its arrangement and serve the isolated effect. In other words, the PP–SiO_2 possesses an interpenetrating structure. It should be mentioned that the melting temperature of PE in PP–SiO_2 did not shift compared with the neat PE-b-PEG, this result indicates that the melting transition PE was not affected by the silica, therefore, it could be inferred that the PE and PP may be immiscible in PP–SiO_2.

Fig. 4 is the XRD pattern of PP–SiO_2 (S3). The first peak ($2\theta = 18.66^\circ$) could be assigned to the PP crystal in PP–SiO_2 [36], and the second and third peaks are attributed to the PE crystal in PE-b-PEG [37]. The shoulder peak from 20° to 25° belongs to the amorphous silica.

The adsorption–desorption hysteresis loop and detailed BET data of PP–SiO_2 (S3) are displayed in Fig. 5 and Table 1 respectively. When the calcined temperature of PP–SiO_2 was 200 °C, the solvent (water and ethanol) volatilized and created some open pores (as shown in Fig. 6), the PE block and the PP were melting at this temperature and flowed into some pores. With the temperature declining after calcined, the melting PE block and PP were frozen in the silica pores and steamed them, leading to some dead end open pores and inter-connected open pores, and hence the BET surface area, pore volume and mean pore size increased slightly. When the calcined temperature increased to 400 °C, the PE block was pyrolysis and the PP was melting, the pores which were steamed by the PE block were emerged, and the structure of the pores between the building blocks were partly converted from the dead end and inter-connected to the passing open structure, therefore the BET surface area and the pore volume enhanced greatly. The mean pore size fall down slightly, from 8.45 nm to 8.04 nm, indicating the mean size of these passing pores between the building blocks were very tinny. Enhanced the temperature to 550 °C, all the organic polymer were pyrolysis and the blocked pores of silica matrix were exposed. The former closed pores between the building blocks were transformed to the open pores, so the BET surface area and pore volume raised obviously and the mean pore size of the pores were reduced almost twice.

The significant changes of the BET surface area and pore size reveal that the pyrolysis of PP and PE-b-PEG discloses numerous nano-channels (open pores) existed inside the silica matrix. The appearance of the pores manifests that the PP and PE-b-PEG may be entrapped in the silica pores, or else the BET surface area will not be increased so greatly.

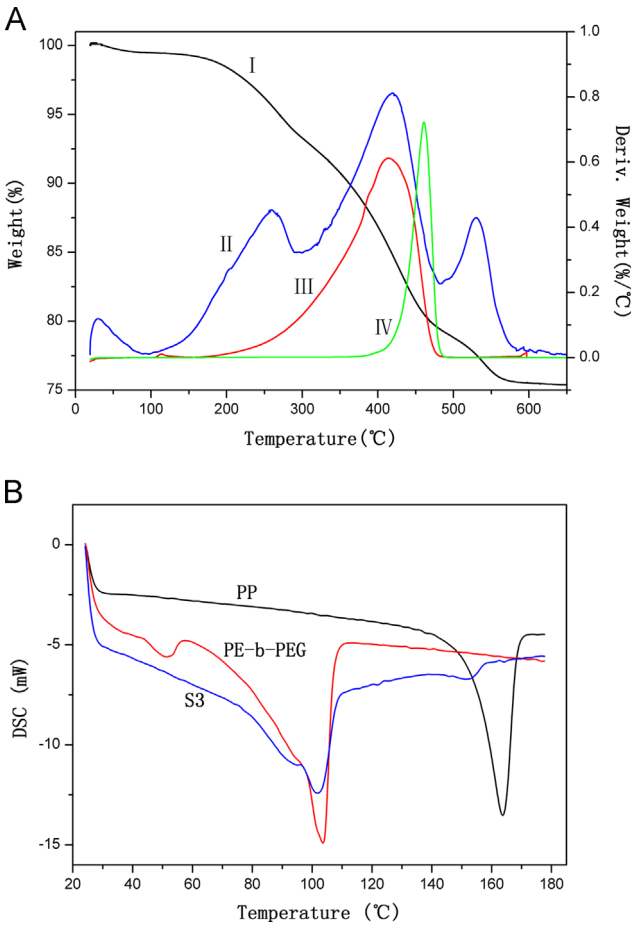

Fig. 3. Thermal properties of the PP–SiO_2. (A) TGA curve of the S3 (I) and DTG curves of the S3 (II), PE-b-PEG (III) and PP (IV). (B) DSC curves of the PP, PE-b-PEG and S3.

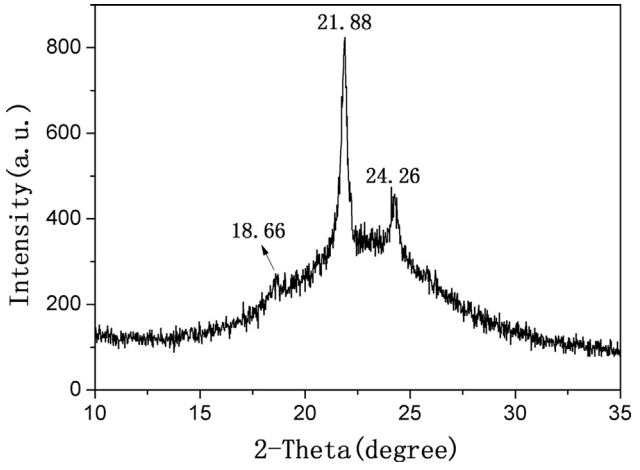

Fig. 4. XRD pattern of the S3.

This conclusion agrees quite well with the results of TGA and DSC measurements.

For the formation mechanism of the interpenetrating structural PP–SiO_2, the formation process includes two stages, as shown in Fig. 7. The first stage is the formation of the stable emulsion. The TEOS was blended with the oil phase (PP, xylene and PE-b-PEG) in advance, when the oil phase was

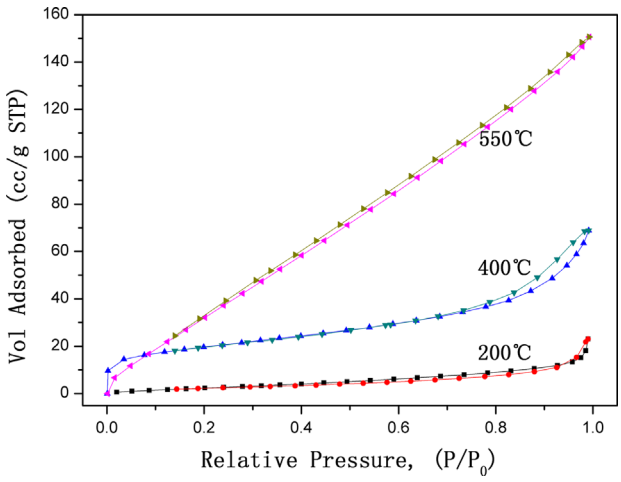

Fig. 5. The adsorption–desorption hysteresis loops of S3.

Table 1
Nitrogen adsorption–desorption experiment data of S3 after calcined at different temperatures.

PP–SiO_2 (°C)	Specific surface area (m^2/g)	Pore volume (cm^3/g)	Mean pore size (nm)
RT	8.9	0.02	6.1
200	12.1	0.04	8.4
400	67.6	0.098	8.0
550	196.7	0.304	4.4

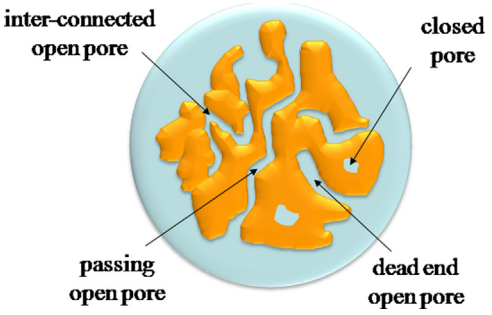

Fig. 6. The schematic illustration of pore structure.

poured into the water phase (ethanol and ammonium hydroxide), the hydrolysis of TEOS was started immediately, and the four hydrophobic Si–OEt bond would partly be converted to the hydrophilic Si–OH bond, so the TEOS could be considered as a surfactant in a way, and together with the PE-b-PEG, to make a stable emulsion. The second stage is the formation of the interpenetrating structure. The hydrolysis and polycondensation of TEOS occurred at the interface between the water phase and oil phase firstly, and then extended to the inner of the oil drops. With the formation of silica matrix, the PP was isolated by the restriction of the silica matrix, and the movement of PP molecule chain would be "frozen" along with the temperature decrement, therefore, the interpenetrating structure formed correspondingly.

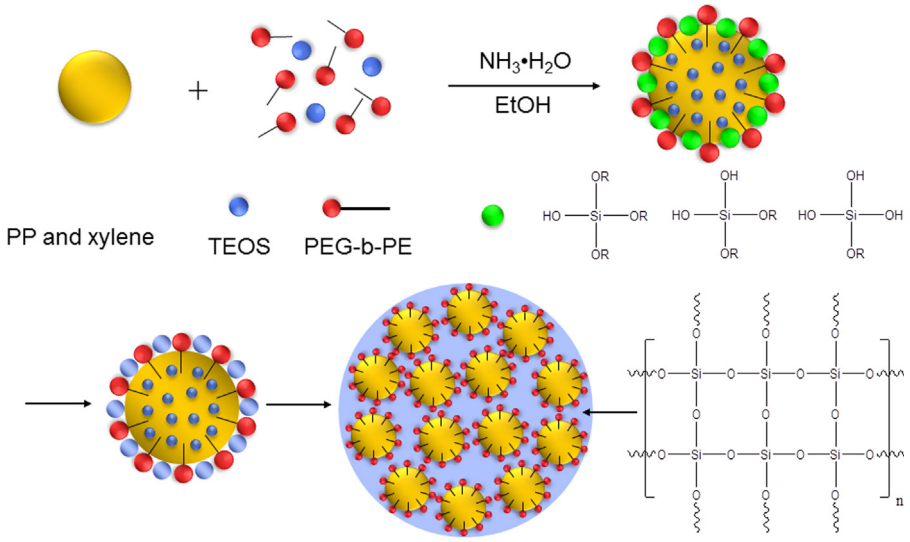

Fig. 7. The schematic illustration of the formation mechanism of PP–SiO_2.

5. Conclusion

The interpenetrating structural PP–SiO_2 nanocomposites were synthesized through a modified sol–gel approach in the presence of the melt polypropylene emulsion in the present investigation. The interpenetrating structure was confirmed by the TGA, DSC and adsorption–desorption measurements results.

1. The PP–SiO_2 particles had irregular particle morphology and the adhesion and aggregation formed among the particles, and the mean particle size of the PP–SiO_2 calculated from the NTA measurements were 150 nm, 168 nm and 172 nm respectively according to the different mass ratio of PP to xylene.
2. The thermal stability of PP was improved significantly, the thermal decomposition temperature was increased to 490 °C, indicating that the thermal decomposition of PP was strongly restricted by inorganic silica walls. The DSC results shown that the melting transition temperature of PP was 151 °C, more than 10 °C lower than neat PP, and the degree of crystallinity is 10.5%.
3. The TGA and DSC results do suggest that the PP and PE-b-PEG were entrapped within the silica matrix, namely, the PP–SiO_2 possess an interpenetrating structure. The nitrogen adsorption–desorption measurement results manifested that the specific surface area and the mean pore volume were increased along with removing the polymer from the PP–SiO_2, which also supported the conclusion obtained from the TGA and DSC results.

Acknowledgments

The authors acknowledge gratefully the support of the National Natural Science Foundation of China (NSFC nos.21271031, 51063009, and 51203012), and the Beijing Natural Science Foundation of China (Nos. 2092013, 2132009, and 2122015).

References

[1] R. Vogel, P.P. Surawski, B.N. Littleton, C.R. Miller, G.A. Lawrie, B.J. Battersby, M. Trau, Fluorescent organosilica micro- and nanoparticles with controllable size, J. Colloid Interface Sci. 310 (2007) 144–150.
[2] B. Fei, H. Lu, J.H. Xin, One-step preparation of organosilica@chitosan crosslinked nanospheres, Polymer 47 (2006) 947–950.
[3] L. Wang, M.C. Estevez, M. O'Donoghu, W. Tan, Fluorophore-free luminescent organosilica nanoparticles, Langmuir 24 (2008) 1635–1639.
[4] A.M. Jakob, T.A. Schmedake, A Novel, Approach to monodisperse, luminescent silica spheres, Chem. Mater. 18 (2006) 3173–3175.
[5] M. Nakamura, M. Shono, K. Ishimura, Synthesis, characterization, and biological applications of multifluorescent silica nanoparticles, Anal. Chem. 79 (2007) 6507–6514.
[6] M. Nakamura, K. Ishimura, One-pot synthesis and characterization of three kinds of thiol–organosilica nanoparticles, Langmuir 24 (2008) 5099–5108.
[7] C.R. Miller, R. Vogel, P.P.T. Surawski, S.R. Corrie, A. Ruhmann, M. Trau, Biomolecular screening with novel organosilica microspheres, Chem. Commun. (2005) 4783–4785.
[8] C.R. Miller, R. Vogel, P.P.T. Surawski, K.S. Jack, S.R. Corrie, M. Trau, Functionalized organosilica microspheres via a novel emulsion-based route, Langmuir 21 (2005) 9733–9740.
[9] M. Nakamura, K. Ishimura, Synthesis and characterization of organosilica nanoparticles prepared from 3-mercaptopropyltrimethoxysilane as the single silica source, J. Phys. Chem. C 111 (2007) 18892–18898.
[10] K. Shin, J.J. Kim, K.D. Suh, A facile process for generating monolithic-structured nano-silica/polystyrene multi-core/shell microspheres by a seeded sol–gel process method, J. Colloid Interface Sci. 350 (2010) 581–585.
[11] N. Kondrashova, E. Saenko, I. Lebedeva, V. Valtsifer, V. Strelnikov, Effect of organic-silane additives on textural–structural properties of mesoporous silicate materials, Microporous Mesoporous Mater. 153 (2012) 275–281.
[12] C.C. Huang, W. Huang, C.S. Yeh, Shell-by-shell synthesis of multi-shelled mesoporous silica nanospheres for optical imaging and drug delivery, Biomaterials 32 (2011) 556–564.

[13] R.-Q. Fu, J.-J. Woo, S.-J. Seo, J.-S. Lee, S.-H. Moon, Covalent organic/inorganic hybrid proton-conductive membrane with semi-interpenetrating polymer network: Preparation and characterizations, J. Power Sources 179 (2008) 458–466.
[14] T.X. Lav, F. Tran-Van, F. Vidal, S. Péralta, C. Chevrot, D. Teyssié, J.V. Grazulevicius, V. Getautis, H. Derbal, J.M. Nunzi, Synthesis and characterization of p and n dopable interpenetrating polymer networks for organic photovoltaic devices, Thin Solid Films 516 (2008) 7223–7229.
[15] S.-H. Rhee, Effect of molecular weight of poly(ε-caprolactone) on interpenetrating network structure, apatite-forming ability, and degradability of poly(ε-caprolactone)/silica nano-hybrid materials, Biomaterials 24 (2003) 1721–1727.
[16] G. Bonilla, M. Martínez, A.M. Mendoza, J.-M. Widmaier, Ternary interpenetrating networks of polyurethane-poly(methyl methacrylate)-silica: preparation by the sol–gel process and characterization of films, Eur. Polym. J. 42 (2006) 2977–2986.
[17] T. Ogoshi, Y. Chujo, Synthesis of poly(vinylidene fluoride) (PVdF)/silica hybrids having interpenetrating polymer network structure by using crystallization between PVdF chains, J. Polym. Sci. Part A: Polym. Chem. 43 (2005) 3543–3550.
[18] C.H. Lee, S.Y. Hwang, J.Y. Sohn, H.B. Park, J.Y. Kim, Y.M. Lee, Water-stable crosslinked sulfonated polyimide–silica nanocomposite containing interpenetrating polymer network, J. Power Sources 163 (2006) 339–348.
[19] I.M. Arafa, M.M. Fares, A.S. Barham, Sol–gel preparation and properties of interpenetrating, encapsulating and blend silica-based urea-formaldehyde hybrid composite materials, Eur. Polym. J. 40 (2004) 1477–1487.
[20] S. Sinha Ray, M. Okamoto, Polymer/layered silicate nanocomposites: a review from preparation to processing, Prog. Polym. Sci. 28 (2003) 1539–1641.
[21] N. Bitinis, M. Hernandez, R. Verdejo, J.M. Kenny, M.A. Lopez-Manchado, Recent advances in clay/polymer nanocomposites, Adv. Mater. 23 (2011) 5229–5236.
[22] Q. Wu, B. Qu, Synergistic effects of silicotungistic acid on intumescent flame-retardant polypropylene, Polym. Degrad. Stab. 74 (2001) 255–261.
[23] M. Doğan, E. Bayramlı, Synergistic effect of boron containing substances on flame retardancy and thermal stability of clay containing intumescent polypropylene nanoclay composites, Polym. Adv. Technol. 22 (2011) 1628–1632.
[24] M. Okubo, H. Hattori, Competitive adsorption of fibrinogen and albumin onto polymer microspheres having hydrophilic/hydrophobic heterogeneous surface structures, Colloid. Polym. Sci. 271 (1993) 1157–1164.
[25] M. Okubo, S. Kamei, Y. Tosaki, K. Fukunaga, T. Matsumoto, Covalent immobilization of trypsin onto poly(2-hydroxyethyl methacrylate)/polystyrene composite microspheres by cyanogen bromide method and its enzymatic activity, Colloid. Polym. Sci. 265 (1987) 957–964.
[26] L.Y. Beaulieu, K.W. Eberman, R.L. Turner, L.J. Krause, J.R. Dahn, Colossal reversible volume changes in lithium alloys, Electrochem. Solid-State Lett. 4 (2001) A137.
[27] L.Y. Beaulieu, K.C. Hewitt, R.L. Turner, A. Bonakdarpour, A.A. Abdo, L. Christensen, K.W. Eberman, L.J. Krause, J.R. Dahn, The electrochemical reaction of li with amorphous Si–Sn alloys, J. Electrochem. Soc. 150 (2003) A149.
[28] R.D. Boyd, S.K. Pichaimuthu, A. Cuenat, New approach to inter-technique comparisons for nanoparticle size measurements; using atomic force microscopy, nanoparticle tracking analysis and dynamic light scattering, Colloids Surf. A: Physicochem. Eng. Asp. 387 (2011) 35–42.
[29] L. Han, C. Gao, X. Wu, Q. Chen, P. Shu, Z. Ding, S. Che, Anionic surfactants templating route for synthesizing silica hollow spheres with different shell porosity, Solid State Sci. 13 (2011) 721–728.
[30] L.L. Hench, J.K. West, The sol–gel process, Chem. Rev. 90 (1990) 33–72.
[31] B. Adamczyk, A. Hess, E. Kemnitz, Magnesium- and iron-doped chromium fluoride/hydroxyfluoride: synthesis, characterization and catalytic activity, J. Mater. Chem. 6 (1996) 1731–1735.
[32] H.L. Frisch, Y.-P. Xue, S. Maaref, G. Beaucage, Z. Pu, J.E. Mark, Pseudo interpenetrating polymer networks and interpenetrating polymer networks of zeolite 13 X and polystyrene and poly(ethyl acrylate), Macromol. Symp. 106 (1996) 147–166.
[33] L. Mandelkern, Crystallization of Polymers, second ed., McGraw-Hill, New York, 1964.
[34] C.L. Jackson, G.B. McKenna, The melting behavior of organic materials confined in porous solids, J. Chem. Phys. 93 (1990) 9002.
[35] C.L. Jackson, G.B. McKenna, The glass transition of organic liquids confined to small pores, J. Non-Cryst. Solids 131–133 (Part 1) (1991) 221–224.
[36] S. Zhu, J. Chen, Y. Zuo, H. Li, Y. Cao, Montmorillonite/polypropylene nanocomposites: mechanical properties, crystallization and rheological behaviors, Appl. Clay Sci. 52 (2011) 171–178.
[37] F.-A. He, L.-M. Zhang, New polyethylene nanocomposites prepared by in-situ polymerization method using nickel a-diimine catalyst supported on organo-modified ZnAl layered double hydroxide, Compos. Sci. Technol. 67 (2007) 3226–3232.